Unified Picture of Near-Edge and Extended X-Ray-Absorption Fine Structure in Low-Z Molecules

J. Stöhr and K. R. Bauchspiess[a]

IBM Research Division, Almaden Research Center, 650 Harry Road, San Jose, California 95120-6099

(Received 8 April 1991)

Self-consistent $X\alpha$ multiple-scattering calculations for N_2 and O_2 reveal a close connection between the prominent multiple-scattering σ^* shape resonances found near threshold and the weak single-scattering extended x-ray-absorption fine-structure (EXAFS) oscillations at higher energy. The σ^* shape resonance may be interpreted as the first, enhanced, EXAFS wiggle while the valence electron potential is found to significantly influence the EXAFS, signifying a breakdown of the conventional picture.

PACS numbers: 33.10.−n, 33.20.Rm, 78.70.Dm

Low-Z molecules consisting of atoms such as carbon, nitrogen, oxygen, and fluorine are characterized by short bond lengths, $\simeq$1.1–1.5 Å, and by the fact that more than half of the total number of electrons in the molecule are involved in chemical bonding. It is the strongly covalent nature of the bonds between such atoms, resulting in myriads of molecules and compounds, which makes them so important in chemistry and related fields such as polymer and surface science. This special electronic structure is also the origin of unusual K-shell x-ray-absorption spectra. In contrast to other forms of matter [1], free, chemisorbed, and polymeric low-Z molecules exhibit near-edge x-ray-absorption fine-structure, or NEXAFS, spectra characterized by giant resonances [2] and extended structures, or EXAFS, that are unusually weak [3–5] and show puzzling disagreements with theory [3,6].

The dramatic difference between the NEXAFS and EXAFS structures in low-Z molecules is usually attributed to different types of scattering processes of the excited photoelectron. In the NEXAFS region the low-energy photoelectron may be trapped or quasitrapped by the molecular potential [7,8] and the resulting wave-function localization in the final state, which may be visualized as multiple scattering of the photoelectron wave or as excitation of the photoelectron to an unfilled molecular orbital [2], leads to a large dipole matrix element and to narrow and intense resonances. In contrast, in the EXAFS region the scattering processes of the excited, high-energy, photoelectron are dominated by the atomiclike potentials of the central and backscattering atoms [9,10], and typically only single-backscattering processes are important. For low-Z molecules the lack of a sizable electronic core of the constituent atoms leads to relatively small backscattering amplitudes at high kinetic energy [9,10] and therefore the EXAFS oscillations are weak. From this conventional picture it is generally believed that NEXAFS is unrelated to EXAFS, i.e., that NEXAFS is "not"-EXAFS. Here we shall give a unified new picture which links the seemingly disjointed energy regimes.

We have utilized the self-consistent $X\alpha$ multiple-scattering (MS) method which is capable of accounting for both the detailed near-edge as well as the extended fine structure. A unified picture emerges which shows the importance of both the *valence* and *core* potential contributions in properly describing the photoelectron scattering processes. Our results explain the failure of conventional EXAFS calculations noted by Yang, Kirz, and Sham [3,6] in terms of the neglect of the valence electron contribution to the scattering potential. We also find a remarkable link between the position of the σ^* shape resonance, commonly encountered in the NEXAFS spectra of low-Z molecules, and the positions of the EXAFS maxima. This leads to a simple picture where the σ^* resonance can be viewed as the first enhanced EXAFS wiggle, independent of whether the σ^* resonance is bound; i.e., its energy is less than the $1s$ ionization potential (IP) as in O_2, or it lies in the continuum as in N_2.

The self-consistent spin unrestricted $X\alpha$ MS calculations employed the transition state method [11]. The molecular potentials were constructed by removing half of a spin-up or spin-down electron from the $1s$ shell of one of the atoms. By adjusting the muffin-tin radii we then demanded that the calculated spin-dependent IP's matched the experimental values [12] of 409.9 eV for N_2 (spin independent) and 543.1 ($^4\Sigma$ ionic state) and 544.2 eV ($^2\Sigma$ ionic state) for O_2. For N_2 the internuclear distance is 1.098 Å and the final atomic muffin-tin radii were 0.630 Å, corresponding to a volume overlap of 1.2%. For O_2 with a bond length of 1.207 Å the atomic muffin-tin radii were about 0.53 Å and hence did not overlap. All calculations employed an $X\alpha$ exchange potential and thus all energy-dependent damping effects which would require the use of a complex exchange potential were neglected. The molecular potential was modified by a Coulomb potential at larger distances [13]. The calculated bound-state transitions were represented by Gaussians with the appropriate experimental widths and areas corresponding to the calculated oscillator strengths. The continuum cross sections were plotted as calculated. For the EXAFS calculations the expansions in angular momenta were terminated at $l_{max}=6$ within the atomic spheres and $l_{max}=11$ elsewhere. This choice followed the criterion $l_{max}\simeq k_{max}R$ [14], with k_{max} representing the largest wave vector of the EXAFS signal and R the radius of the respective muffin-tin spheres. Convergence of the results was verified by calculations with larger l_{max} values over limited high-energy ranges. Because of the weakness and low frequency of the EXAFS in the calcu-

lated cross section σ it was difficult to extract the EXAFS oscillations by conventional background subtraction techniques. We therefore used a calculated background σ_0, obtained by replacing the core potential of the backscattering atom by the constant interstitial potential. The EXAFS signal was then defined as $\sigma - \sigma_0$ divided by the K-edge jump.

Our calculated results for the NEXAFS spectra of N_2 and O_2 are compared in Fig. 1 to experimental spectra obtained by inner-shell electron-energy-loss spectroscopy [15]. Clearly the overall agreement is very good. For N_2 the remaining discrepancy between theory and experiment can be attributed to multielectron effects [7] which give rise to a structure near 415 eV, shown shaded, and diminish the size of the σ^* resonance, relative to our one-electron calculation. For O_2 the splitting and relative intensity of the σ^* resonance is not reproduced quantitatively, as discussed elsewhere [16].

Experimental EXAFS spectra recorded by Yang, Kirz, and Sham [3] are compared with calculated spectra in Fig. 2. The intensities of the π^* and σ^* resonances are distorted by sample thickness effects [6], but this does not affect the EXAFS structure which is clearly seen after background subtraction. The experimental and calculated EXAFS oscillations for O_2 taken from Fig. 2, including the low-energy σ^* resonance, are directly compared on a wave-vector scale in Fig. 3. The zero of the energy and wave-vector scales was chosen to coincide with the bottoms of the muffin-tin wells, located 29.2 eV for O_2 and 25.8 eV for N_2 below the vacuum level. In contrast to the results of conventional EXAFS theory plotted by Yang, Kirz, and Sham [3] the positions of the EXAFS wiggles calculated by us are in much better agreement with experiment. Here it is important to note that we have found that the discrepancy between experiment and the plane-wave theory of Teo and Lee [9] cannot be eliminated by inclusion of curved-wave effects [10]. On the other hand, our results for O_2 in the $k \geq 4$ Å^{-1} region are in good agreement with those obtained by Rehr [17] using a single-scattering curved-wave theory that realistically accounts for charge overlap of the valence electrons in the construction of the scattering potential [18]. As expected, these latter calculations fail, however, in the NEXAFS region, owing to the neglect of multiple scattering. The discrepancy between measured and calculated amplitudes above 5 Å^{-1} is attributed to the omission of inelastic multielectron effects in our theory. In the 3–5-Å^{-1} range shakeoff structure (dashed shading) is directly evident in the experimental data.

In Fig. 3 we also show calculations of the extended fine structure for N_2 for which, unfortunately, no published experimental data exist. As for O_2, a pronounced σ^* resonance is followed by much weaker EXAFS. Because of the shorter bond length in N_2 the EXAFS wiggles are stretched and the spacing between the maxima increases. The most interesting result is indicated by a bar diagram below the respective curves revealing nearly equal intervals between the positions of the σ^* resonance and the

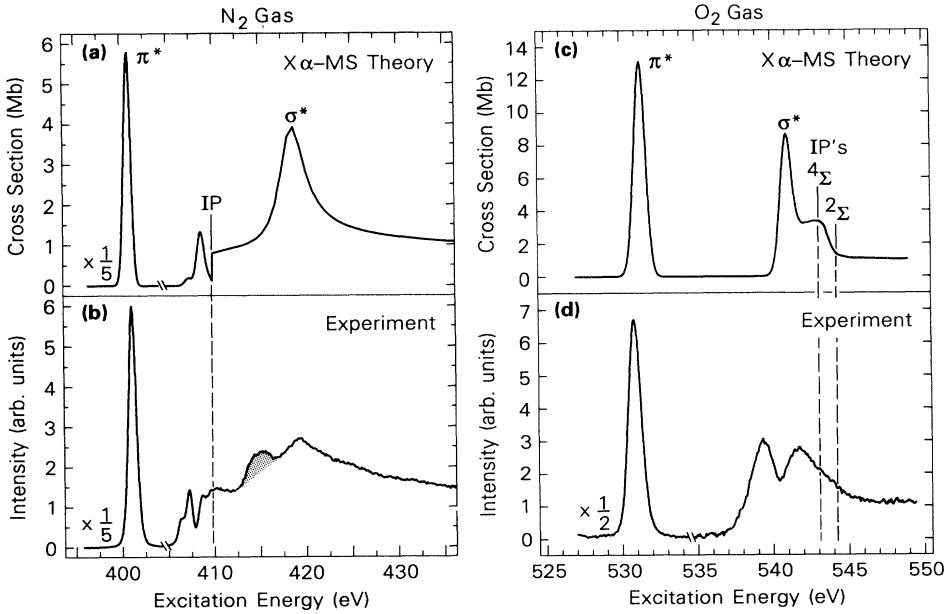

FIG. 1. (a) NEXAFS spectrum of N_2 calculated by means of $X\alpha$ multiple-scattering theory compared to that (b) measured by inner-shell electron-energy-loss spectroscopy [15]. The 1s ionization potential is marked IP, and the shaded resonance in (b) is a multielectron feature. (c) Calculated and (d) experimental [15] NEXAFS spectra for O_2. Because O_2 is paramagnetic there are two IP's and the σ^* resonance is magnetically split [16]. Note that the σ^* resonance lies in the continuum for N_2 but is bound for O_2. All resonances below the IP have been convoluted with a Gaussian of 0.9 eV width.

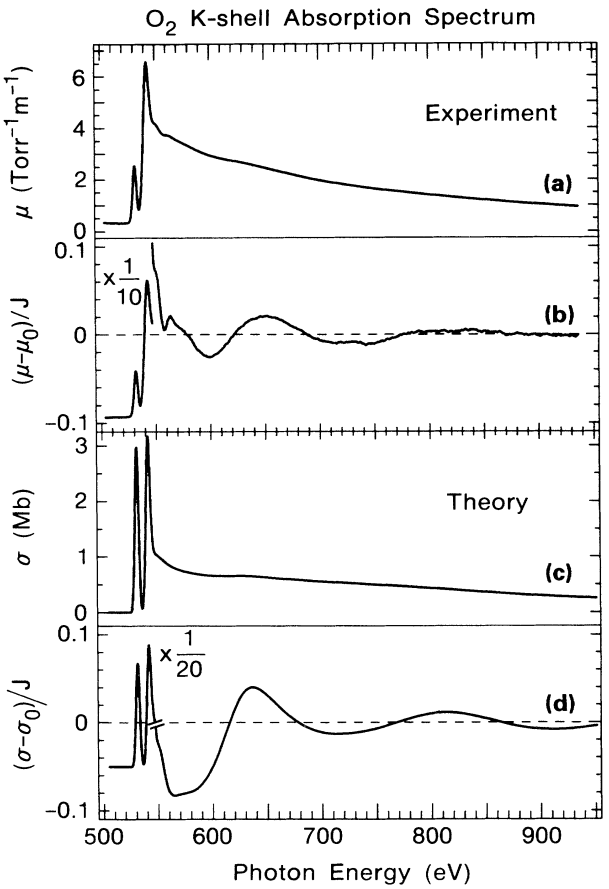

FIG. 2. (a) Experimental K-shell x-ray-absorption coefficient μ of free O_2 [3]. Note that the intensities of the π^* and σ^* resonances at 531 and 541 eV are distorted due to a sample-thickness effect. (b) Absorption fine structure $(\mu-\mu_0)/J$, *where* μ_0 is a smooth background function and J is the edge jump. (c) X-ray-absorption cross section σ calculated by means of $X\alpha$ MS theory. The widths of the calculated π^* and σ^* bound-state resonances have been convoluted with a Gaussian of 4.0 eV width to match the experimental width. (d) Calculated absorption fine structure $(\sigma-\sigma_0)/J$, where σ_0 has been calculated as discussed in the text.

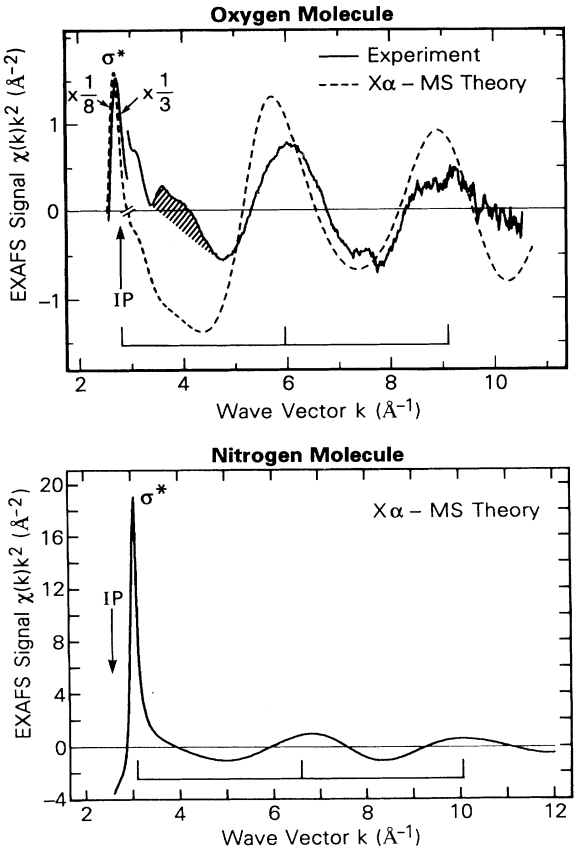

FIG. 3. K-shell x-ray-absorption structure $\chi(k)k^2$ for O_2 and N_2 as a function of wave vector k. For O_2 the calculation is compared with the experimental data (solid line) of Yang, Kirz, and Sham [3] and the σ^* resonance intensity near $k=2.7$ Å^{-1} is reduced by factors of 3 and 8 for the experimental and theoretical curves, respectively. For O_2 the energy zero for our wave-vector scale calculation was 514.4 eV. This value lies by 29.2 eV, the calculated interstitial potential, below the average $1s$ IP (543.65 eV). For N_2, the energy zero was chosen at 384.1 eV, 25.8 eV below the $1s$ IP (409.9 eV).

EXAFS maxima for both O_2 and N_2. Thus by extrapolation of the EXAFS maxima to lower wave vectors one is naturally led to the position of the σ^* resonance, which may therefore be associated with the first EXAFS maximum whose intensity is enhanced by multiple scattering.

The origin of the correlation implied by the bar diagram in Fig. 3 may be understood from inspection of the scattering potential of the O_2 molecule shown in Fig. 4. The potential has two main components, a "molecular" well centered between the atoms, with a radius that is roughly equal to the bond length and a depth given by the interstitial potential, and "atomic" wells at the nuclear positions. The molecular well is largely determined by the valence-electron charge distribution and its bottom defines the zero of the kinetic energy of the photoelectron [8] and therefore the zero of the EXAFS scale. One important conclusion from our calculations is that for low-Z molecules *both wells are important for the quantitative description of the scattering processes in the NEXAFS and the EXAFS regions.*

The positions of the σ^* NEXAFS resonances are not simply determined by the valence-electron potential but the core potentials have an important effect. This is the reason for the correspondence of the σ^* resonance position with that of the first EXAFS wiggle found here and the previously established "EXAFS-like" dependence of the σ^* resonance position on bond length [8,19]. For the EXAFS structure the reverse is true. In conventional EXAFS calculations [9,10] the molecular well arising from the detailed *valence-electron* charge distribution is neglected. Its effect is assumed to be small at high kinetic energies of the photoelectron and taken into account at

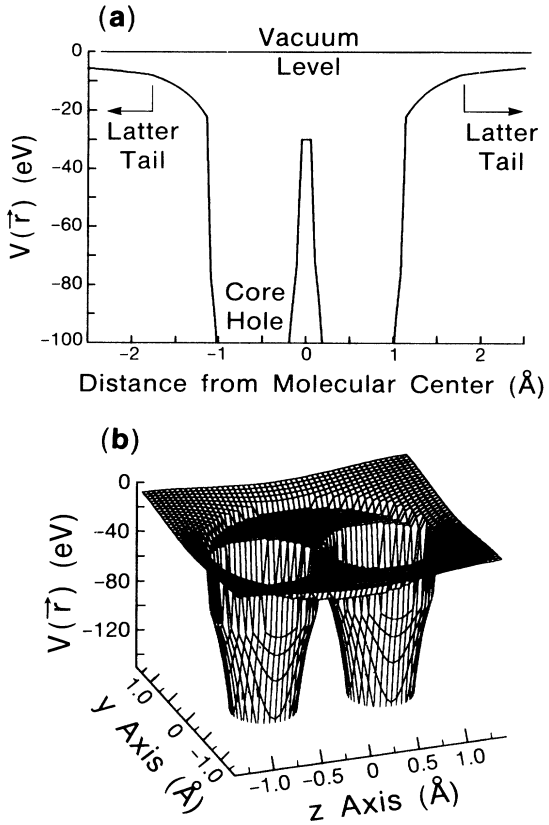

FIG. 4. $X\alpha$ molecular potential for the spin-up electrons in the O_2 molecule. (a) Cut of the potential in the plane containing the nuclei. For distances larger than 1.75 Å from the molecular center the $X\alpha$ potential has been substituted by a Coulomb potential, marked "Latter tail." (b) Three-dimensional plot of the potential. The nuclei are located at $y=0$ and $z=\pm 0.604$ Å.

lower kinetic energies by adjustment of the zero of the EXAFS energy and wave-vector scale. Because of the large depth of this well for low-Z molecules this approximation breaks down. The molecular well causes a large phase-shift correction relative to the phase shift obtained with atomiclike potentials. This correction is found to be nearly constant over the experimentally accessible EXAFS range in good accord with the empirical observations by Yang, Kirz, and Sham [3,6].

Our results also explain previous observations made for low-Z solids. In graphite, diamond [20], and solid benzene and cyclohexane [4] unusually large corrections (30–40 eV) of the zero of energy value were required in conjunction with Teo and Lee's [9] theoretical C-C phase shifts. In the above systems the bonding between adjacent C atoms leads to a non-negligible valence-electron contribution to the effective scattering potential, as for O_2 and N_2. On the other hand, Teo and Lee's phase shifts were found to describe the O-O EXAFS in solid H_2O [21]. In this case the EXAFS signal arises from scattering events involving oxygen atoms that are not bonded together and separated by a rather large distance (2.76 Å). As a consequence, the scattering potentials for the central and backscattering atoms are atomiclike and no corrections of published phase shifts [9,10] are needed.

We are grateful to John Horsley for providing the $X\alpha$ MS programs, to John Rehr for many useful discussions and sharing unpublished EXAFS results, to Adam Hitchcock for the O_2 and N_2 NEXAFS data, and to B. X. Yang and J. Kirz for the O_2 EXAFS data.

[a]Present address: Photon Factory, National Laboratory for High Energy Physics, 1-1 Oho, Tsukuba-shi, Ibaraki-ken 305, Japan.

[1] *Principles, Applications, Techniques of EXAFS, SEXAFS, and XANES*, edited by D. C. Koningsberger and R. Prins (Wiley, New York, 1988).
[2] J. Stöhr, *NEXAFS Spectroscopy*, Springer Series in Surface Sciences (Springer, Heidelberg, 1991).
[3] B. X. Yang, J. Kirz, and T. K. Sham, Phys. Rev. A **110**, 301 (1985).
[4] G. Comelli and J. Stöhr, Surf. Sci. **200**, 35 (1988).
[5] B. P. Hollebone, A. T. Wen, T. Tyliszczak, and A. P. Hitchcock, J. Electron Spectrosc. **51**, 661 (1990).
[6] B. X. Yang, J. Kirz, and T. K. Sham, Phys. Rev. A **36**, 4298 (1987).
[7] J. L. Dehmer and D. Dill, Phys. Rev. Lett. **35**, 213 (1975); J. Chem. Phys. **65**, 5327 (1976).
[8] C. R. Natoli, in *EXAFS and Near Edge Structure*, edited by A. Bianconi, L. Incoccia, and S. Stipcich, Springer Series in Chemical Physics Vol. 27 (Springer, New York, 1983), p. 43.
[9] B. K. Teo and P. A. Lee, J. Am. Chem. Soc. **101**, 2815 (1978).
[10] A. G. McKale, B. W. Veal, A. P. Paulikas, S.-K. Chan, and G. S. Knapp, J. Am. Chem. Soc. **110**, 3763 (1988).
[11] J. C. Slater and K. H. Johnson, Phys. Rev. B **5**, 844 (1972).
[12] W. L. Jolly, K. D. Bomben, and C. J. Eyermann, At. Data Nucl. Data Tables **31**, 433 (1984).
[13] R. Latter, Phys. Rev. **99**, 510 (1955).
[14] L. I. Schiff, *Quantum Mechanics* (McGraw-Hill, New York, 1968), 3rd ed., Sec. 19.
[15] A. P. Hitchcock and C. E. Brion, J. Electron Spectrosc. **18**, 1 (1980); A. P. Hitchcock (private communication).
[16] W. Wurth, J. Stöhr, P. Feulner, X. Pan, K. R. Bauchspiess, Y. Baba, E. Hudel, G. Rocker, and D. Menzel, Phys. Rev. Lett. **65**, 2426 (1990).
[17] J. J. Rehr (private communication).
[18] J. Mustre de Leon, J. J. Rehr, S. I. Zabinsky, and R. C. Albers, Phys. Rev. B **44**, 4146 (1991).
[19] J. Stöhr, J. L. Gland, W. Eberhardt, D. Outka, R. J. Madix, F. Sette, R. J. Koestner, and U. Döbler, Phys. Rev. Lett. **51**, 2414 (1983); F. Sette, J. Stöhr, and A. P. Hitchcock, J. Chem. Phys. **81**, 4906 (1984).
[20] G. Comelli, J. Stöhr, W. Jark, and B. Pate, Phys. Rev. B **37**, 4383 (1988).
[21] R. A. Rosenberg, P. R. LaRoe, V. Rehn, J. Stöhr, R. Jaeger, and C. C. Parks, Phys. Rev. B **28**, 3026 (1983).